Spin-orbit coupled fermions in ladderlike optical lattices at half filling

G. Sun, J. Jaramillo, L. Santos, and T. Vekua*
Institut für Theoretische Physik, Leibniz Universität Hannover, 30167 Hannover, Germany
(Received 17 July 2013; published 2 October 2013)

We study the ground-state phase diagram of two-component fermions loaded in a ladderlike lattice at half filling in the presence of spin-orbit coupling. For repulsive fermions with unidirectional spin-orbit coupling along the legs we identify a Néel state which is separated from rung-singlet and ferromagnetic states by Ising phase transition lines. These lines cross for maximal spin-orbit coupling and a direct Gaussian phase transition between rung-singlet and ferro phases is realized. For the case of Rashba-like spin-orbit coupling, besides the rung-singlet phases two distinct striped ferromagnetic phases are formed. In the case of attractive fermions with spin-orbit coupling at half filling for decoupled chains we identify a dimerized state that separates a singlet superconductor and a ferromagnetic state.

DOI: 10.1103/PhysRevB.88.165101 PACS number(s): 05.30.Fk, 03.75.Ss, 03.75.Mn, 71.10.Fd

I. INTRODUCTION

The possibility of inducing synthetic electromagnetism in ultracold gases has recently attracted a great deal of attention. In spite of the electric charge neutrality of an atom, a synthetic magnetic field may be induced by a proper laser arrangement.[1] Interestingly, unidirectional spin-orbit coupling (USOC) resulting from an equal superposition of Rashba[2] and linear Dresselhaus[3] terms has been realized for both spinor Bose[4] and Fermi gases[5,6] with the help of counter-propagating Raman lasers. Recently this technique has allowed for observation of the superfluid Hall effect,[7] Zitterbewegung,[8] and the spin-Hall effect in a quantum gas.[9] Several theoretical works have discussed the creation of pure Rashba or Dresselhaus spin-orbit coupling (SOC) by optical[10] and magnetic means[11] and even proposed methods to generate three-dimensional (3D) SOC.[12]

The presence of synthetic SOC is expected to lead to rich physics for atoms loaded in optical lattices. For 2D Hubbard models at half filling the effects of Rashba-like SOC were studied both for two-component bosons and fermions, for which exotic spin textures in the ground state such as coplanar spiral waves and stripes as well as noncoplanar vortex/antivortex configurations have been predicted.[13–16] Note, however, that the SOC introduces frustration, invalidating quantum Monte Carlo (MC) approaches, and hence most studies have relied on classical MC calculations.

In this paper we analyze the effects of SOC in a two-component Fermi gas loaded in an optical lattice in the Mott-insulator regime. Since we are interested in the quantum spin-1/2 phases in the presence of SOC, we cannot rely on classical MC and, hence, must employ exact diagonalization or density-matrix renormalization-group (DMRG) techniques. We employ the latter in this paper, restricting our analysis to the minimal system where the non-Abelian character of the vector potential may be manifested, allowing nontrivial effects of SOC without the need to break the time-reversal invariance, namely, a two-leg ladderlike optical lattice, which may be created by incoherently combining a 1D lattice and a two-well potential. By a combination of numerical DMRG results, bosonization techniques, and strong rung-coupling expansions, we obtain the spin quantum phases for both USOC with different orientations with respect to the ladder and isotropic SOC.

The paper is organized as follows. In Sec. II we introduce the effective spin model for a Mott state of two-component fermions with USOC in a ladderlike lattice. In Sec. III we review the phases for the case of decoupled 1D lattices. Section IV deals with the quantum phases of USOC discussing the different orientations between the USOC and the ladder legs. In Sec. V we analyze the case of isotropic SOC. We, finally, summarize in Sec. VI.

II. EFFECTIVE SPIN MODEL FOR TWO-COMPONENT FERMIONS WITH USOC

Recent experiments have realized USOC characterized by a Hamiltonian of the form[4]

$$H_{\mathrm{USOC}} = \frac{1}{2m}(\mathbf{p}\sigma^0 - \mathbf{A})^2 + \frac{\delta}{2}\sigma^z - \frac{h}{2}\sigma^x, \qquad (1)$$

where $\sigma^{z,x}$ are Pauli matrices, σ^0 is the identity matrix, and the effective vector potential for counter-propagating Raman lasers on the xy plane is given by $\mathbf{A} = -\hbar\mathbf{k}_0\sigma^z$, with $\mathbf{k}_0 = (k_0^x, k_0^y, 0)$. Here the eigenvectors of σ^z correspond to atomic hyperfine components, the term $\frac{\delta}{2}\sigma^z$ is due to detuning from resonance, and h is the Rabi coupling. Crucially, $\mathbf{A}$ cannot be completely gauged out, since it does not commute with the scalar potential $\Phi = \frac{\delta}{2}\sigma^z - \frac{h}{2}\sigma^x$.

We consider a two-component Fermi gas loaded in a ladderlike optical lattice of intersite spacing a, with the ladder legs oriented along x and the rungs along y. Projecting on the lowest lattice band[17] one obtains, in the absence of SOC, the two-component Fermi-Hubbard model,

$$H_{\mathrm{FH}} = -\sum_{(i,i'),\sigma,\sigma'} t_{i,i'}\sigma^0_{\sigma,\sigma'} a^\dagger_{i,\sigma} a_{i',\sigma'} + \frac{U}{2}\sum_i n_i(n_i - 1), \qquad (2)$$

where $a_{i,\sigma}$ is the annihilation operator of fermions with spin $\sigma = \uparrow,\downarrow$ on site i, $n_i = \sum_\sigma a^\dagger_{i,\sigma} a_{i,\sigma}$, U characterizes the on-site interaction, and $t_{i,i'}$ are the hopping amplitudes along the bonds connecting nearest-neighbor sites (i,i'), with the hopping along the legs (the rungs) given by $t_{i,i'} = t_x$ (t_y). The presence of SOC results in the Peierls substitution $t_{i,i'}\sigma^0 \to t_{i,i'} e^{i\frac{\mathbf{A}(\mathbf{r}_{i'} - \mathbf{r}_i)}{\hbar}}$. In the strong-coupling limit, $U \to \infty$, and considering half filling (i.e., we consider a Mott phase with one fermion per site),[18,19] the Fermi-Hubbard model may

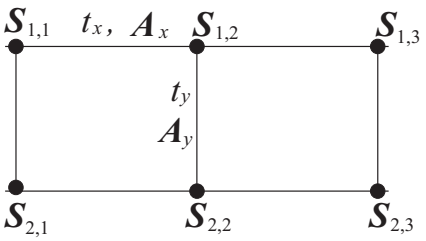

FIG. 1. Two-leg ladder lattice of $s = 1/2$ spins $\mathbf{S}_{\alpha,j}$, where $\alpha = 1,2$ enumerates the ladder legs, and $j = 1,2,3,\ldots,L$ labels the ladder rungs.

be rewritten as an effective spin-1/2 model of the form

$$\begin{aligned} H = J_\parallel \sum_{\alpha,j} \{ & \cos\left(2k_0^x a\right)\mathbf{S}_{\alpha,j}\mathbf{S}_{\alpha,j+1} + 2\sin^2\left(k_0^x a\right) S^z_{\alpha,j} S^z_{\alpha,j+1} \\ & + \sin\left(2k_0^x a\right)[\mathbf{S}_{\alpha,j} \times \mathbf{S}_{\alpha,j+1}]^z \} \\ & + J_\perp \sum_j \{ \cos\left(2k_0^y a\right)\mathbf{S}_{1,j}\mathbf{S}_{2,j} + 2\sin^2\left(k_0^y a\right) S^z_{1,j} S^z_{2,j} \\ & + \sin 2k_0^y a[\mathbf{S}_{1,j} \times \mathbf{S}_{2,j}]^z \} + \delta \sum_{\alpha,j} S^z_{\alpha,j} - h \sum_{\alpha,j} S^x_{\alpha,j}, \end{aligned} \tag{3}$$

where $J_\parallel = 4t_x^2/U$, $J_\perp = 4t_y^2/U$, and

$$\mathbf{S}_{\alpha,j} = (a^\dagger_{\alpha,j,\uparrow}, a^\dagger_{\alpha,j,\downarrow}) \frac{\boldsymbol{\sigma}}{2} \begin{pmatrix} a_{\alpha,j,\uparrow} \\ a_{\alpha,j,\downarrow} \end{pmatrix} \tag{4}$$

are the spin operators associated with the leg $\alpha = 1,2$ and rung j (see Fig. 1), with the site index i in Eq. (2) split into leg and rung indices: $i \to (\alpha, j)$. The value of k_0^x and k_0^y is provided by the orientation between the Raman lasers creating the USOC and the ladder axis. Note that the scalar potential Φ produces the last two terms in Eq. (3), whereas the vector potential $\mathbf{A}$ produces Dzyaloshinskii-Moriya terms,[21,22] $\sim[\mathbf{S}_{\alpha,j} \times \mathbf{S}_{\alpha',j'}]^z$, as well as easy-axis anisotropy along $\mathbf{e}_z$.

III. DECOUPLED CHAINS

A. Repulsive interactions

We first discuss the case of decoupled chains, $J_\perp = 0$ (i.e., $t_y = 0$), which results in the 1D Hamiltonian

$$\begin{aligned} H_{1D} = J_\parallel \sum_j & \left(S^z_j S^z_{j+1} + \cos 2k_0^x a \left(S^x_j S^x_{j+1} + S^y_j S^y_{j+1}\right)\right. \\ & \left. + \sin 2k_0^x a \left(S^x_j S^y_{j+1} - S^y_j S^x_{j+1}\right)\right) - h \sum_j S^x_j. \end{aligned} \tag{5}$$

For $k_x^0 = 0$, Eq. (5) describes an SU(2)-symmetric spin-1/2 antiferromagnetic chain in an external magnetic field, which is exactly solvable by means of the Bethe ansatz.[23] The ground state is a gapless Luttinger liquid (LL) for $h < 2J_\parallel$, and a fully polarized state for $h > 2J_\parallel$. These two phases are separated by a commensurate-incommensurate (C-IC) phase transition.

In order to discuss the effects of USOC it is convenient to introduce a gauge transformation that renders exchange interactions explicitly SU(2) invariant, $H_{1D} \to U H_{1D} U^\dagger = \bar{H}_{1D}$, where $U = \prod_j e^{-2ik_0^x a j S^z_j}$. The spin operators

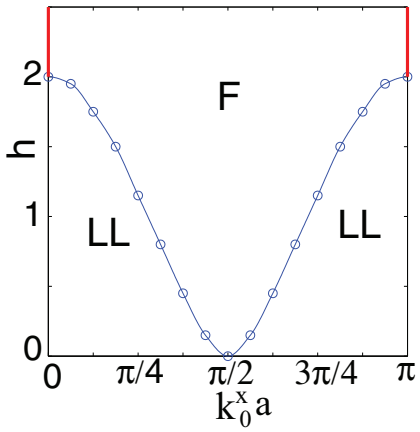

FIG. 2. (Color online) Ground states of a 1D spin-1/2 chain with USOC and a transverse magnetic field obtained using DMRG for 96 sites. The magnetic field is in units of $J_\parallel$. LL, Luttinger liquid phase; F, ferromagnetic state.

transform as

$$\begin{aligned} \bar{S}^x_j &= \cos\left(2k_0^x a j\right) S^x_j - \sin\left(2k_0^x a j\right) S^y_j, \\ \bar{S}^y_j &= \cos\left(2k_0^x a j\right) S^y_j + \sin\left(2k_0^x a j\right) S^x_j, \end{aligned} \tag{6}$$

and $\bar{S}^z_j = S^z_j$, and the Hamiltonian becomes

$$\bar{H}_{1D} = J_\parallel \sum_j \bar{\mathbf{S}}_j \bar{\mathbf{S}}_{j+1} - \sum_j \mathbf{h}_j(\mathbf{k}_0)\bar{\mathbf{S}}_j, \tag{7}$$

where the effect of the USOC is entirely absorbed into an external magnetic field, $\mathbf{h}_j(\mathbf{k}_0) = h(\cos(2k_0^x a j), \sin(2k_0^x a j), 0)$, which spirals on the xy plane.

For $k_0^x a = \pi/2$, $\mathbf{h}_j = (-1)^j h\, \mathbf{e}_x$, i.e., a staggered effective magnetic field. A staggered field constitutes a relevant perturbation (in the renormalization-group sense) as it couples to the Néel order, which is one of the leading instabilities in a 1D antiferromagnetic chain. As a result of this, a gap in the excitation spectrum, $\Delta E \sim h^{2/3}$, opens for any arbitrary coupling h. The low-energy behavior is described by a massive sine-Gordon model where one of the breather modes is degenerate with soliton and antisoliton excitations.[24] In the gauge-transformed variables the ground state develops Néel order, which, after undoing the gauge transformation, results for the original spin operators in an uniformly magnetized state, i.e., a ferromagnetic (F) state, although magnetization is never fully saturated for $k_0^x \neq 0$.

For $0 < k_0^x a < \pi/2$, $\mathbf{h}_j(\mathbf{k}_0)$ is IC and hence the gapless LL phase survives up to a finite h value at which the F phase is reached. We have employed the matrix product formulation[26] of the DMRG method[27,28] to obtain numerically the phase diagram for arbitrary values of the USOC (see Fig. 2). This phase diagram confirms the existence of a gapless LL and a gapped F phase separated by a C-IC transition. Note that correlation functions, which decay algebraically in the LL phase and exponentially in the F phase, are generically incommensurate due to the Dzyaloshinskii-Moriya anisotropy, and the vector product of two neighboring spins has finite expectation value $\langle[\mathbf{S}_j \times \mathbf{S}_{j+1}]^z\rangle \sim -\sin(2k_0^x a)$ as depicted in Fig. 3(a). Its magnetic-field dependence is presented in Fig. 3(b). We note that $\langle[\mathbf{S}_j \times \mathbf{S}_{j+1}]^z\rangle$ serves as an order

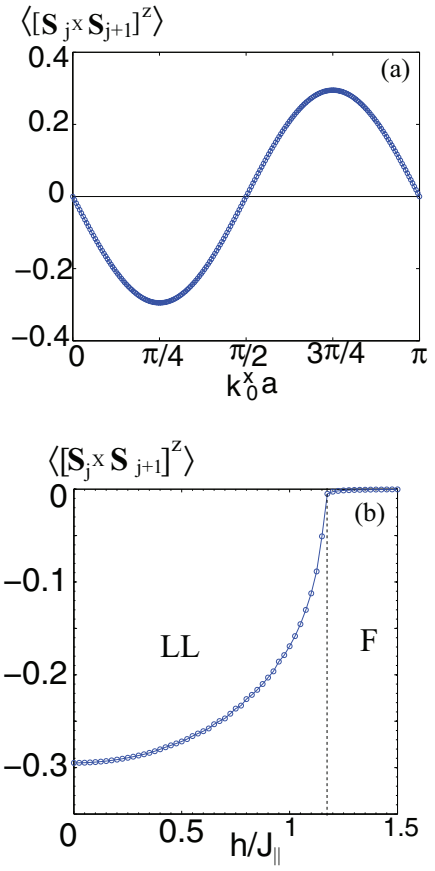

FIG. 3. (Color online) Expectation value of the vector product of two neighboring spins obtained by DMRG simulations for 96 sites as a function of (a) the USOC parameter, $k_0^x a$, for $h = 0$ and (b) the magnetic field for $k_0^x a = \pi/4$.

parameter that is nonzero in the LL phase and vanishes rapidly in the F phase, showing cusplike behavior at the C-IC phase transition indicated by the dashed line in Fig. 3(b).

B. Attractive interactions

For decoupled chains we have also studied the case of two-component fermions with attractive interactions. The most interesting ground-state physics occurs at half filling in the vicinity of the maximal USOC, $k_0^x a \simeq \pi/2$. In this case, after particle-hole transformation the 1D Fermi-Hubbard model becomes dual to the repulsive ionic-Hubbard model,[25] being characterized by the existence of a dimerized (D) phase between a superconducting phase and the F state. With increasing magnetic field the superconducting phase undergoes a Kosterlitz-Thouless transition into the D state, where translational symmetry is spontaneously broken. Further increasing the magnetic field results in a D-F Ising transition. We characterized the D phase in our numerical simulations by means of the dimerization order parameter, which, in a chain with L sites, is defined as

$$D = \sum_j \frac{(-1)^j}{L} \langle a^\dagger_{j,\uparrow} a_{j+1,\downarrow} - a^\dagger_{j,\downarrow} a_{j+1,\uparrow} + \text{H.c.} \rangle. \quad (8)$$

The phase diagram of the 1D attractive Fermi-Hubbard model with $k_0^x a = \pi/2$ at half filling is presented in Fig. 4.

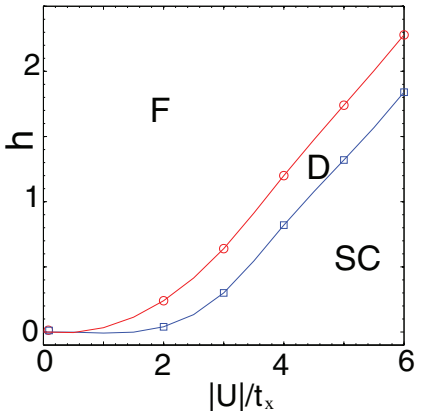

FIG. 4. (Color online) Phase diagram for an attractive two-component Fermi-Hubbard model on a chain at half filling with maximal USOC. D, dimerized phase; SC, 1D superconductor. The magnetic field is in units of t_x. Phase boundaries are obtained after finite-size extrapolation from data obtained for 128, 256, 512, and 1024 sites.

IV. TWO-LEG LADDER WITH USOC

We consider now the case of coupled chains with nonzero hoppings $t_{x,y}$. As mentioned above, the value of k_x^0 and k_y^0 depends on the orientation of the USOC lasers and the ladder axis. In the following we consider separately the case in which the USOC is along the rungs and that in which the USOC is along the legs.

A. USOC along the ladder rungs

We analyze first the case of an USOC along the ladder rungs (Fig. 5); i.e., $k_0^x = 0$ in Eq. (3). For $k_0^y = 0$ the magnetic field introduces two C-IC phase transitions: from a rung-singlet (RS) into an LL and then from the LL into the fully polarized F state. As in our discussion in Sec. III it is convenient to introduce the gauge transformation,

$$\begin{aligned} \bar{S}^x_{\alpha,j} &= \cos\left(2k_0^y a\alpha\right) S^x_{\alpha,j} - \sin\left(2k_0^y a\alpha\right) S^y_{\alpha,j}, \\ \bar{S}^y_{\alpha,j} &= \cos\left(2k_0^y a\alpha\right) S^y_{\alpha,j} + \sin\left(2k_0^y a\alpha\right) S^x_{\alpha,j}, \end{aligned} \quad (9)$$

and $\bar{S}^z_{\alpha,j} = S^z_{\alpha,j}$. For the case of the maximal USOC, $k_0^y a = \pi/2$, the gauge-transformed Hamiltonian becomes

$$\bar{H} = J_\parallel \sum_{\alpha=(1,2),j} \bar{\mathbf{S}}_{\alpha,j} \bar{\mathbf{S}}_{\alpha,j+1} + J_\perp \sum_j \bar{\mathbf{S}}_{1,j} \bar{\mathbf{S}}_{2,j} - h \sum_{\alpha=(1,2),j} (-1)^\alpha \bar{S}^x_{\alpha,j}. \quad (10)$$

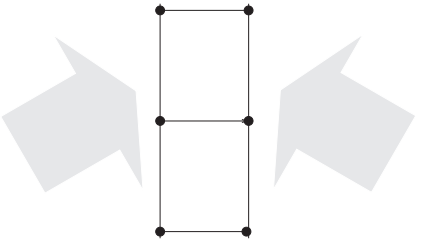

FIG. 5. Raman lasers counter-propagating along ladder rungs result in USOC as discussed in Sec. IV A.

In the strong-rung-coupling limit, $J_\perp \gg J_\parallel$, the ground state becomes a rung-product state of the form

$$|\bar{RS}\rangle = \prod_j (|\bar{\uparrow}_{1,j}\rangle \otimes |\bar{\downarrow}_{2,j}\rangle - \beta|\bar{\downarrow}_{1,j}\rangle \otimes |\bar{\uparrow}_{2,j}\rangle)/\sqrt{1+\beta^2}, \tag{11}$$

where $\{\bar{\uparrow},\bar{\downarrow}\}$ refer to the eigenstates of $\bar{S}^x$. For $h = 0$, $\beta = 1$ and the ground state is a product state of singlets along the rungs. With increasing magnetic field, β decreases, gradually tending to 0. For $\beta = 0$ the ground state after undoing the gauge transformation translates into the F state. Hence, for $k_0^y a = \pi/2$ the magnetic field just results in an adiabatic evolution of $|\bar{RS}\rangle$ into the F state.

To address the general case $0 < k_0^y < \pi/2$ we consider the case of weak USOC, $k_0^y a \ll 1$, closely following the strong-rung-coupling derivation in Ref. 29. For $h = 0$ the ground state is well approximated by a direct product of singlets along the rungs, and the energy gap to the lowest rung triplet excitation is $\sim J_\perp$. The external magnetic field splits the rung triplet excitations linearly, and the energy of the state where both spins of the rung point in the direction of the field approaches that of the RS state for $h \sim J_\perp$. Identifying the RS state on a rung with an effective spin-1/2 pointing down, and the $S^x = 1$ component of the rung triplet state with the spin-1/2 pointing up, the effective pseudo-spin-1/2 model in the strong-rung-coupling limit for $h \sim J_\perp$ takes the form of an XXZ model in a tilted uniform magnetic field,

$$H_\tau = J_\parallel \sum_j \left(\frac{1}{2}\tau_j^x \tau_{j+1}^x + \tau_j^y \tau_{j+1}^y + \tau_j^z \tau_{j+1}^z\right) - h_x \sum_j \tau_j^x - h_y \sum_j \tau_j^y, \tag{12}$$

where $\tau^{x,y,z}$ are the pseudo-spin-1/2 operators, $h_x = h - J_\perp \cos 2k_0^y a + J_\perp(1 - \cos 2k_0^y a)/4 - J_\parallel/2$, and $h_y = J_\perp \sin 2k_0^y a/\sqrt{2}$. With varying h_x model (12) undergoes changes in three ground-state phases:[30] two F phases separated by Ising transitions from an intermediate Néel phase in the τ^z state. One of the F phases of the effective model, (12), translates to the RS phase of the ladder, whereas the Néel phase and the second F phase of (12) translate into identical ladder phases. Note that it is the Dzyaloshinskii-Moriya interaction that, in the leading order, breaks in Eq. (12) the U(1) rotation symmetry in the yz plane allowing for the Néel ordering.

We consider at this point weakly coupled chains, $J_\perp \ll J_\parallel$, again for weak USOC, $k_0^y a \ll 1$, where bosonization provides an exact effective (low-energetic) description[31] with the convention

$$\begin{aligned} S_{\alpha,j}^x &\to \frac{\partial_x \phi_\alpha}{\sqrt{2\pi}} + (-1)^j \sin\sqrt{2\pi}\phi_\alpha, \\ S_{j,\alpha}^y &\to (-1)^j \sin\sqrt{2\pi}\theta_\alpha + \cdots, \\ S_{\alpha,j}^z &\to (-1)^j \cos\sqrt{2\pi}\theta_\alpha + \cdots, \end{aligned} \tag{13}$$

where $x = ja$, the ellipses denote subleading fluctuations of uniform components, and we have introduced two pairs of dual bosonic fields, $[\theta_\alpha(x), \partial_y \phi_{\alpha'}] = i\delta_{\alpha,\alpha'}\delta(x-y)$. It is convenient to introduce the symmetric and antisymmetric combinations of the original bosonic fields, $\theta_\pm = (\theta_1 \pm \theta_2)/\sqrt{2}$ and $\phi_\pm = (\phi_1 \pm \phi_2)/\sqrt{2}$. We treat $J_\perp$ as a perturbation of the two decoupled chains, retaining only the relevant contributions that it generates. We obtain the Hamiltonian density

$$\begin{aligned} \mathcal{H}_B = &\sum_{\nu=\pm} \frac{v_\nu}{2}[(\partial_x \phi_\nu)^2 + (\partial_x \theta_\nu)^2] - h\partial_x \phi_+/\sqrt{\pi} \\ &+ \tilde{J}_\perp(2\cos\sqrt{4\pi}\theta_- - \cos\sqrt{4\pi}\phi_+ + \cos\sqrt{4\pi}\phi_-) \\ &+ \tilde{d}_\perp(\cos\sqrt{\pi}\phi_+ \sin\sqrt{\pi}\theta_+ \sin\sqrt{\pi}\phi_- \cos\sqrt{\pi}\theta_- \\ &- \sin\sqrt{\pi}\phi_+ \cos\sqrt{\pi}\theta_+ \cos\sqrt{\pi}\phi_- \sin\sqrt{\pi}\theta_-) \\ &+ d_\perp(\cos\sqrt{4\pi}\theta_- + \cos\sqrt{4\pi}\theta_+), \end{aligned} \tag{14}$$

where

$$v_\pm \simeq \frac{J_\parallel a\pi}{2}\left(1 \pm \frac{J_\perp \cos(2k_0^y a)}{J_\parallel \pi^2}\right)$$

and $\tilde{J}_\perp \sim J_\perp \cos(2k_0^y a)$. Dzyaloshinskii-Moriya anisotropy generates the terms with the coupling constant $\tilde{d}_\perp \sim J_\perp \sin(2k_0^y a)$, whereas easy-axis anisotropy induces the terms with the prefactor $d_\perp \sim J_\perp(1 - \cos(2k_0^y a))$. All three factors, $\tilde{J}_\perp$, $\tilde{d}_\perp$, and $d_\perp$, depend as well on a short-distance cutoff. Note that the magnetic field, h, just couples to the symmetric sector.

For $k_0^y a \ll 1$, $d_\perp, \tilde{d}_\perp \ll \tilde{J}_\perp$, and the antisymmetric sector remains gapped with $\langle\theta_-\rangle = \sqrt{\pi}/2$. Note that when the magnetic field suppresses the dominant coupling in the symmetric sector, $\tilde{J}_\perp \cos\sqrt{4\pi}\phi_+$, the easy-axis anisotropy term induces the leading instability.

The symmetric sector can be solved by means of Jordan-Wigner mapping and a subsequent Bogoliubov transformation. It supports two Ising phase transitions with increasing magnetic field that separate three different ground-state phases. In the original spin variables, these phases translate into the RS phase, a Néel state with order parameter $n = (-1)^{j+\alpha}\langle S_{\alpha,j}^z\rangle \neq 0$, and the F phase. In the Néel state spins are canted uniformly along the applied field as depicted in Fig. 6.

We recall that for $k_0^y a = \pi/2$ a growing magnetic field does not introduce any phase transition but rather adiabatically connects RS and F phases. Since in the vicinity of $k_y^0 a = 0$ an intermediate Néel phase occurs, we expect, as a function of $k_0^y a$ and h, the presence of a Néel island inside an overall RS-F state. Our numerical results confirm this expectation, as depicted in Fig. 7. Since Néel order is spontaneous, in our numerical calculations we monitor

$$n^2 \equiv \lim_{|i-j|\gg 1} \left|(-1)^{i-j}\langle S_{\alpha,i}^z S_{\alpha,j}^z\rangle\right|. \tag{15}$$

The magnetic-field dependence of n^2 is illustrated in Fig. 8(a).

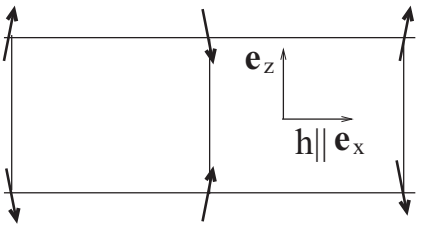

FIG. 6. Néel-state configuration for USOC along rungs. The interleg correlation functions are also antiferromagnetic, $\langle S_{1,i}^z S_{2,j}^z\rangle \sim (-1)^{i-j+1}$.

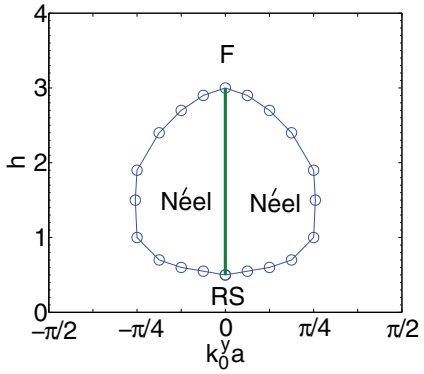

FIG. 7. (Color online) Phase diagram for USOC along ladder rungs. The phase transition curve into the Néel state is determined from the closing of the gap between the two lowest eigenstates; see Fig. 8(b). For $k_0^y = 0$ an LL line is realized between the RS and the F phases. The magnetic field is in units of $J_\parallel = J_\perp$.

We have also studied the behavior of the excitation gap. The Néel state is characterized by a doubly degenerate ground state in the thermodynamic limit, whereas the RS and F states have unique gapped ground states. Hence a simple way to obtain the boundary of the Néel state is to follow the closing of the gap between the ground state and the first excited state (that becomes degenerate with the ground state in the thermodynamic limit in the Néel phase). We plot the behavior of the gap in Fig. 8(b). The gaps close linearly with the magnetic field when approaching the quantum phase transition points, as expected from the Ising character.

We note, finally, that the vector product of two neighboring spins has a finite expectation value along rungs,

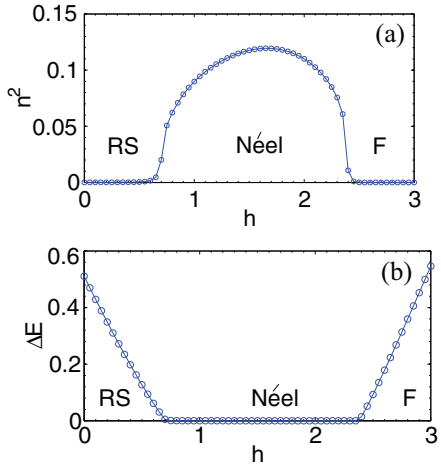

FIG. 8. (Color online) (a) Square Néel order as a function of the magnetic field along a cut through the RS-Néel-F phases for $k_0^x = 0$ and $k_0^y = \pm 3\pi/16$. (b) Behavior of the energy gap between the two lowest eigenstates as a function of the magnetic field across the RS-Néel-F phases. The Néel state is characterized by doubly degenerate ground states. The magnetic field and the gap are both measured in units of $J_\parallel = J_\perp$. Depicted results correspond to DMRG simulations with $L = 48$ rungs. Finite-size effects near both phase transitions are very similar to the behavior depicted in Figs. 10(a) and 10(b) close to the Néel-to-F transition.

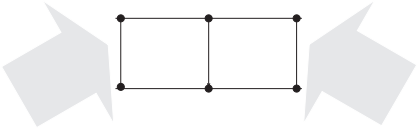

FIG. 9. Raman lasers counter-propagating along the ladder legs result in USOC like that discussed in Sec. IV B. The value of k_x^0 can be controlled by the angle between the laser propagation direction and the ladder legs.

$\langle [\mathbf{S}_{1,j} \times \mathbf{S}_{2,j}]^z \rangle \sim -\sin(2k_0^y a)$, in all phases, becoming 0 only deep in the F phase for large values of h.

B. Two-leg ladder with USOC along the legs

We consider now that the USOC is oriented along the ladder legs, as depicted in Fig. 9, and hence $k_0^y = 0$ in Eq. (3). For $k_0^x = 0$, the external magnetic field induces two consecutive C-IC phase transitions: the first from the RS into the gapless LL phase and the second from the LL into the fully polarized F state. For $k_x^0 \neq 0$ we may perform a gauge transformation similar to those discussed above, which, for the maximal USOC, $k_0^x a = \pi/2$, results in a model similar to Eq. (10), but in this case with a field that couples uniformly to spins belonging to the same rung and alternates from rung to rung, $-h \sum_{\alpha,j} (-1)^j \bar{S}^x_{\alpha,j}$. Using bosonization in the weak-rung-coupling limit, $J_\perp \ll J_\parallel$, and in the opposite limit, $J_\perp \gg J_\parallel$, employing strong-rung-coupling expansion it has been determined that such a magnetic field introduces Gaussian criticality between two gapped phases of the antiferromagnetic spin ladder,[33] which, for our original spin variables, corresponds to the RS and F states.

The difference at maximal USOC between the case with USOC along the ladder legs and that with USOC along the rungs can be easily understood in the limit $J_\perp \gg J_\parallel$. For the case of USOC along the ladder legs the magnetic field couples uniformly to the spins on the same rung, and hence it favors a triplet state on each rung, with both spins pointing in the same direction, which alternates from one rung to the next. This state is orthogonal to the RS configuration. In contrast, in Eq. (10) the magnetic field couples in a staggered way to the spins in the same rung, and the ground state favored by a strong magnetic field is not orthogonal to the RS state. As a result, for the USOC along rungs the RS state can be adiabatically connected to the F state, whereas for the USOC along legs this is not possible.

Based on the previous discussion we expect that the two C-IC phase transition points for $k_0^x a = 0$ have to evolve into a single Gaussian point for $k_0^x a = \pi/2$. As for the case of USOC along rungs, we can employ bosonization to understand this evolution of the critical points in the limit $J_\perp \ll J_\parallel$. The leading instability once the magnetic field suppresses the RS phase is again the easy-axis anisotropy, however, now in exchange interactions along the chains, and Dzyaloshinskii-Moriya anisotropy induces incommensurability.[34] In contrast to the relevant couplings produced by USOC along the rungs, in Eq. (14) USOC along ladder legs produces a marginal perturbation, $\sim \cos\sqrt{4\pi}\theta_- \cos\sqrt{4\pi}\theta_+$. After mean-field decoupling between the symmetric and the antisymmetric sectors the weak-rung-coupling bosonic Hamiltonian for USOC along

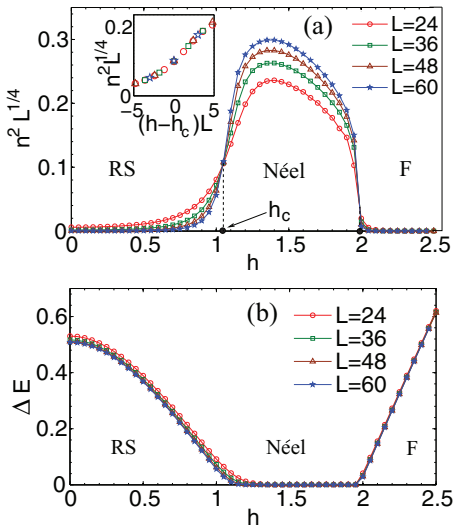

FIG. 10. (Color online) (a) Square Néel order, n^2, as a function of the magnetic field along a cut through the RS-Néel-F phases for $k_0^x = \pi/4$ and $k_y^0 = 0$ and for different system sizes. Inset: Collapse of our numerical results for different system sizes on a single curve according to the Ising scaling. (b) Behavior of the energy gap between the two lowest eigenstates as a function of the magnetic field across the RS-Néel-F phases. The Néel state is characterized by doubly degenerate ground states. The magnetic field and the gap are measured in units of $J_\parallel = J_\perp$. Results displayed correspond to DMRG simulations for $L = 24$, 36, 48, and 60 rungs.

the legs is equivalent to Eq. (14), and hence the ground states and phase transitions will be similar to the previous case of USOC along the rungs. Thus C-IC phase transition points evolve into Ising lines for $k_0^x a > 0$, and at $k_x^0 a = \pi/2$ these two Ising lines merge in a Gaussian criticality due to the enhanced symmetry.

Our numerical results for n^2 and the excitation gap are depicted in Fig. 10. Note that finite-size effects are more pronounced at the RS-to-Néel transition, whereas for the Néel-to-F transition finite-size effects are negligible. For the RS-to-Néel transition we have carefully performed finite-size scaling of the order parameter and determined the critical field h_c corresponding to the phase transition from the intersection of the order parameter curves for different system sizes. The collapse of the order parameter for different system sizes in the vicinity of h_c on the single curve according to the Ising law is depicted in the inset in Fig. 10(a).

Note, finally, that the vector product of two neighboring spins has finite expectation value along the chains $\langle [\mathbf{S}_{\alpha,j} \times \mathbf{S}_{\alpha,j+1}]^z \rangle \sim -\sin(2k_0^x a)$. Its magnetic-field dependence is similar to the curve in Fig. 3(b), and it vanishes quickly in the F phase.

The ground-state phase diagram for USOC along the ladder legs is depicted in Fig. 11. As mentioned above, the C-IC phase transition points [corresponding to U(1) symmetry at $k_0^x = 0$] transform into Ising transitions (for $0 < k_0^x < \pi/2$ the system does not have continuous symmetry), and then they combine into a Gaussian point at $k_0^x a = \pi/2$ [where U(1) symmetry is revived].

So in both cases, USOC along the ladder rungs and along the ladder legs, the system presents three possible phases: RS, Néel, and F. For a general orientation of the USOC and the ladder legs, $k_0^x \neq 0$ and $k_0^y \neq 0$, we hence expect these three phases as well.

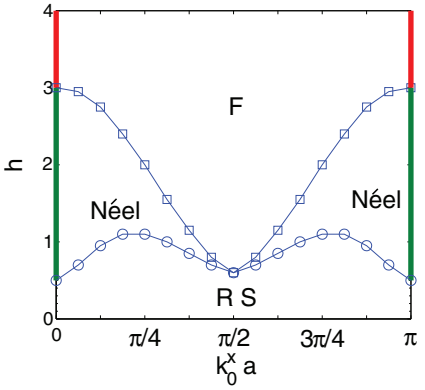

FIG. 11. (Color online) Numerical phase diagram for USOC along the ladder legs, $k_0^y = 0$. For $k_0^x = 0(\pi)$ there are two C-IC transitions with increasing magnetic field: the first from RS to LL and the second from the LL into the fully polarized state (both LL and fully polarized states are indicated by bold lines). For $0 < k_0^x < \pi/2$, instead of the LL state a Néel state is realized, being separated from the RS and F states by Ising phase transition lines. These lines cross at $k_0^x = \pi/2$, resulting in a direct Gaussian transition from RS to F. The magnetic field is in units of $J_\parallel = J_\perp$. Phase boundaries are obtained for the system with $L = 48$ rungs.

V. TWO-LEG LADDER WITH A NON-ABELIAN VECTOR POTENTIAL

We consider at this point a non-Abelian vector potential of the form $\mathbf{A} = (-\hbar k_0^x \sigma^x, -\hbar k_0^y \sigma^y)$. Contrary to the case of USOC, the magnetic field, h, is not necessary to ensure the nontrivial character of SOC. We hence consider the time-reversal symmetric case, $h = 0$, and a balanced mixture of up- and down-spin fermions. Effects of a magnetic field in a quarter filled Fermi Hubbard model with Rashba interaction was studied in Ref. 35. The effective spin model in this case acquires the form

$$\begin{aligned} H = {} & J_\parallel \sum_{\alpha,j} \{ \cos(2k_0^x a) \mathbf{S}_{\alpha,j} \mathbf{S}_{\alpha,j+1} + 2\sin^2(k_0^x a) S^x_{\alpha,j} S^x_{\alpha,j+1} \\ & + \sin(2k_0^x a) [\mathbf{S}_{\alpha,j} \times \mathbf{S}_{\alpha,j+1}]^x \} \\ & + J_\perp \sum_j \{ \cos(2k_0^y a) \mathbf{S}_{1,j} \mathbf{S}_{2,j} + 2\sin^2(k_0^y a) S^y_{1,j} S^y_{2,j} \\ & + \sin(2k_0^y a) [\mathbf{S}_{1,j} \times \mathbf{S}_{2,j}]^y \}. \end{aligned} \quad (16)$$

Our numerical results for the ground-state phase diagram are presented in Fig. 12. In the vicinity of zero SOC, $k_0^x a = k_0^y a = 0$, the system is in the RS state. For the case of maximal SOC, $k_0^x a = k_0^y a = \pi/2$, we may employ the canonical transformation $\mathbf{S}_{\alpha,i} \to \tilde{\mathbf{S}}_{\alpha,i} = U \mathbf{S}_{\alpha,i} U^\dagger$, with

$$U = \prod_j e^{-i\pi S^y_{1,j}} \prod_{\alpha,k=2j} e^{-i\pi S^x_{\alpha,k}}, \quad (17)$$

which transforms Hamiltonian (16) into an SU(2) symmetric antiferromagnetic spin ladder Hamiltonian of the form of Eq. (10) with $h = 0$.

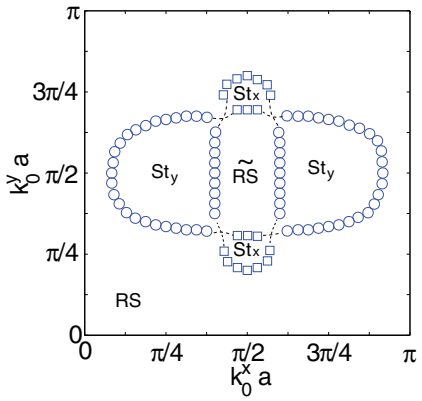

FIG. 12. (Color online) Ground states for a spin ladder with Rashba SOC (see text). Numerical results correspond to DMRG calculations for $L = 48$ rungs.

Thus for $k_0^x a = k_0^y a = \pi/2$ the system is in the RS phase but in the gauge-transformed spins (hence we denote it $\widetilde{\text{RS}}$), with no long-range order and exponentially decaying correlation functions. In the strong rung coupling limit the ground state in gauge transformed variables is the RS product state Eq. (11) with $\beta = 1$, that for original variables transforms via U to the direct product of $S^z = 0$ components of the rung triplets, also of the form of Eq. (11), but with $\beta = -1$. Since the $\widetilde{\text{RS}}$ state is gapped it will occupy a finite region around the $k_0^x a = k_0^y a = \pi/2$ point.

In the RS phase the vector product of two neighboring spins has finite expectation value: along the chains $\langle[\mathbf{S}_{\alpha,j} \times \mathbf{S}_{\alpha,j+1}]^x\rangle \sim -\sin(2k_0^x a)$, and along the rungs $\langle[\mathbf{S}_{1,j} \times \mathbf{S}_{2,j}]^y\rangle \sim -\sin(2k_0^y a)$. In the $\widetilde{\text{RS}}$ phase the vector product of two neighboring spins is negligibly small.

Our numerical results also reveal the appearance of striped phases with long-range order where spins are ferromagnetically ordered in one direction and antiferromagnetically in the other. The case of F order along the rung (St_y phase) is best understood in the vicinity of the $(k_0^x a, k_0^y a) = (\pi/4, \pi/2)$ point, where $\cos(2k_0^x a) = 0$, and $\cos(2k_0^y a) = -1$. For these parameters the coupling along the rung $S^x_{1,j} S^x_{2,j}$ is F, whereas the intra-leg coupling $S^x_{\alpha,j} S^x_{\alpha,j+1}$ is antiferromagnetic, which results in the St_y configuration observed in our numerical calculations (Fig. 13).

We may understand in a similar way the appearance of the St_x phase (see Fig. 14), analyzing the behavior in the vicinity of $(k_0^x a, k_0^y a) = (\pi/2, \pi/4)$, which is characterized by

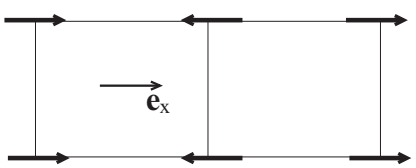

FIG. 13. St_y-state configuration of a two-leg ladder with Rashba SOC. Spins are oriented along the $\pm\mathbf{e}_x$ direction on odd rungs and along $\mp\mathbf{e}_x$ on even rungs. In the St_y state the vector products of nearest-neighbor spins behave as $\langle[\mathbf{S}_{\alpha,j} \times \mathbf{S}_{\alpha,j+1}]^x\rangle \sim -\sin(2k_0^x a)$ and $\langle[\mathbf{S}_{1,j} \times \mathbf{S}_{2,j}]^y\rangle \sim 0$. In the plot of the St_y state a nonzero value of the $\langle[\mathbf{S}_{\alpha,j} \times \mathbf{S}_{\alpha,j+1}]^x\rangle$ quantity is not reflected.

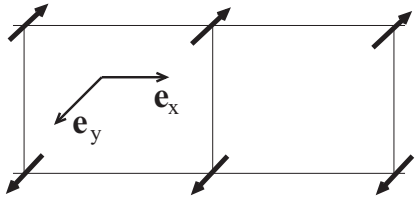

FIG. 14. St_x-phase configuration of a two-leg ladder with Rashba SOC. Spins are oriented along the $\pm\mathbf{e}_y$ direction on one leg and along $\mp\mathbf{e}_y$ on the other. In the St_x phase the vector products of nearest-neighbor spins behave as $\langle[\mathbf{S}_{\alpha,j} \times \mathbf{S}_{\alpha,j+1}]^x\rangle \sim 0$ and along rungs $\langle[\mathbf{S}_{1,j} \times \mathbf{S}_{2,j}]^y\rangle \sim -\sin(2k_0^y a)$.

an F $S^y_{\alpha,j} S^y_{\alpha,j+1}$ coupling along legs and an antiferromagnetic $S^y_{1,j} S^y_{2,j}$ exchange along rungs. The St_x and St_y states are dual to each other with respect to the interchange of leg and rung directions and S^x and S^y components. Our numerical simulations suggest that, similarly to the USOC case, all phase transitions for the case of the non-Abelian vector potential are of second-order Ising nature. This is natural, since the system does not enjoy, in general, any continuous symmetry, and striped phases break spontaneously discrete Z^2 symmetries: St_y breaks translation symmetry along the chains direction, whereas St_x breaks the parity symmetry associated with the exchange of ladder legs. Both striped phases also break time-reversal symmetry.

The RS and $\widetilde{\text{RS}}$ phases present different parity symmetry for an odd number of rungs, where the RS phase is antisymmetric and the $\widetilde{\text{RS}}$ is symmetric; as a result, these two phases can not be connected adiabatically with each other. We could not determine numerically whether the RS and $\widetilde{\text{RS}}$ states can be connected adiabatically for an even number of rungs in the parameter space (k_0^x, k_0^y) in Fig. 12. In particular, the string order, defined for the pair of spins across the ladder diagonal, is finite for both the RS and the $\widetilde{\text{RS}}$ states and vanishes in the striped phases. However, in the thermodynamic limit we expect the behaviors of odd and even numbers of rungs to converge, and hence it is most likely that in the model given in Eq. (16) the RS and $\widetilde{\text{RS}}$ states are always separated by a phase transition (indicated by dashed lines in Fig. 12).

VI. CONCLUSIONS

In this work we have discussed the quantum spin phases and the associated quantum phase transitions for a two-component Fermi lattice gas, focusing on the case of a two-leg ladderlike lattice at half filling, a minimal system to study the non-Abelian character of the vector potential. We have shown that for USOC along the ladder rungs the Néel-state phase is located within the RS-F phase, in which an RS may be adiabatically connected to an F phase in the parameter space of h and the SOC. In contrast, for USOC along the ladder legs the RS and F states cannot be adiabatically connected and are separated by an intermediate Néel state, which disappears at maximal SOC to lead to a direct Gaussian RS-F quantum phase transition. The case of Rashba-like SOC is characterized by the appearance of RS and striped phases. Compared to the classical spin phases predicted for fermions on a square lattice with SOC,[15] only the

striped configurations of the 2D lattice have identical quantum counterparts on the ladder. On the contrary, the Néel and spiral waves are substituted by gapped RS states, whereas noncoplanar configurations such as vortex/antivortex textures are not stabilized.

The Néel and striped phases show long-range magnetic order, thus they can be observed experimentally in ultracold spinor Fermi gases with artificial SOC[5,6] by Bragg diffraction of light,[36] provided that cooling is achieved below the spin degeneracy temperature. The RS and F states have no long-range order, though they can be revealed by probing the local order similarly to recent experiments in Ref. 37; e.g., two sites on the same rung will show antiferromagnetic superexchange interaction in the RS state and F correlation in the F state.

ACKNOWLEDGMENTS

We thank A. K. Kolezhuk and S. Manmana for discussions. This work was supported by QUEST (Center for Quantum Engineering and Space-Time Research) and DFG Research Training Group (Graduiertenkolleg) 1729.

*vekua@itp.uni-hannover.de

[1] Y.-J. Lin, R. L. Compton, K. Jimenez-Garcia, J. V. Porto, and I. B. Spielman, Nature **462**, 628 (2009).
[2] Y. A. Bychkov and E. I. Rashba, J. Phys. C **17**, 6039 (1984).
[3] G. Dresselhaus, Phys. Rev. **100**, 580 (1955).
[4] Y.-J. Lin, K. Jimenez-Garcia, and I. B. Spielman, Nature **471**, 83 (2011).
[5] P. Wang, Z. Q. Yu, Z. Fu, J. Miao, L. Huang, S. Chai, H. Zhai, and J. Zhang, Phys. Rev. Lett. **109**, 095301 (2012).
[6] L. W. Cheuk, A. T. Sommer, Z. Hadzibabic, T. Yefsah, W. S. Bakr, and M. W. Zwierlein, Phys. Rev. Lett. **109**, 095302 (2012).
[7] L. J. LeBlanc *et al.*, Proc. Natl. Acad. Sci. USA **109**, 10811 (2012).
[8] L. J. LeBlanc, M. C. Beeler, K. Jiménez-García, A. R. Perry, S. Sugawa, R. A. Williams, and I. B. Spielman, New J. Phys. **15**, 073011 (2013).
[9] M. C. Beeler *et al.*, Nature **498**, 201 (2013).
[10] D. L. Campbell, G. Juzeliunas, and I. B. Spielman, Phys. Rev. A **84**, 025602 (2011).
[11] B. M. Anderson, I. B. Spielman, and G. Juzeliunas, arXiv:1306.2606.
[12] B. M. Anderson, G. Juzeliunas, V. M. Galitski, and I. B. Spielman, Phys. Rev. Lett. **108**, 235301 (2012).
[13] Z. Cai, X. Zhou, and C. Wu, Phys. Rev. A **85**, 061605(R) (2012).
[14] W. S. Cole, S. Zhang, A. Paramekanti, and N. Trivedi, Phys. Rev. Lett. **109**, 085302 (2012).
[15] J. Radic, A. Di Ciolo, K. Sun, and V. Galitski, Phys. Rev. Lett. **109**, 085303 (2012).
[16] M. Gong, Y. Qian, V. W. Scarola, and C. Zhang, arXiv:1205.6211.
[17] D. Jaksch, C. Bruder, J. I. Cirac, C. W. Gardiner, and P. Zoller, Phys. Rev. Lett. **81**, 3108 (1998).
[18] R. Jördens, N. Strohmaier, K. Günter, H. Moritz, and T. Esslinger, Nature (London) **455**, 204 (2008).
[19] U. Schneider *et al.*, Science **322**, 1520 (2008).
[20] R. Jördens *et al.*, Phys. Rev. Lett. **104**, 180401 (2010).
[21] I. Dzyaloshinskii, J. Phys. Chem. Solids **4**, 241 (1958).
[22] T. Moriya, Phys. Rev. **120**, 91 (1960).
[23] M. Takahashi, *Thermodynamics of One-Dimensional Solvable Models* (Cambridge University Press, Cambridge, UK, 1999).
[24] M. Oshikawa and I. Affleck, Phys. Rev. Lett. **79**, 2883 (1997).
[25] M. Fabrizio, A. O. Gogolin, and A. A. Nersesyan, Phys. Rev. Lett. **83**, 2014 (1999); A. P. Kampf, M. Sekania, G. I. Japaridze, and P. Brune, J. Phys.: Condens. Matter **15**, 5895 (2003); S. R. Manmana, V. Meden, R. M. Noack, and K. Schönhammer, Phys. Rev. B **70**, 155115 (2004).
[26] F. Verstraete, J. J. Garcia-Ripoll, and J. I. Cirac, Phys. Rev. Lett. **93**, 207204 (2004).
[27] S. R. White, Phys. Rev. Lett. **69**, 2863 (1992); Phys. Rev. B **48**, 10345 (1993).
[28] U. Schollwöck, Rev. Mod. Phys. **77**, 259 (2005).
[29] K. Penc, J. B. Fouet, S. Miyahara, O. Tchernyshyov, and F. Mila, Phys. Rev. Lett. **99**, 117201 (2007).
[30] A. A. Ovchinnikov, D. V. Dmitriev, V. Y. Krivnov, and V. O. Cheranovskii, Phys. Rev. B **68**, 214406 (2003); D. V. Dmitriev and V. Y. Krivnov, *ibid.* **70**, 144414 (2004); J.-S. Caux, F. H. L. Essler, and U. Löw, *ibid.* **68**, 134431 (2003).
[31] A. O. Gogolin, A. A. Nersesyan, and A. M. Tsvelik, *Bosonization and Strongly Correlated Systems* (Cambridge University Press, Cambridge, UK, 1998).
[32] Y.-J. Wang, arXiv:cond-mat/0306365v1; F. H. L. Essler and I. Affleck, J. Stat. Mech. (2004) P12006.
[33] Y.-J. Wang, F. H. L. Essler, and M. Fabrizio, and A. A. Nersesyan, Phys. Rev. B **66**, 024412 (2002).
[34] R. Citro and E. Orignac, Phys. Rev. B **65**, 134413 (2002).
[35] J. A. Riera, Phys. Rev. B **88**, 045102 (2013).
[36] T. A. Corcovilos, S. K. Baur, J. M. Hitchcock, E. J. Mueller, and R. G. Hulet, Phys. Rev. A **81**, 013415 (2010).
[37] D. Greif, T. Uehlinger, G. Jotzu, L. Tarruell, and T. Esslinger, Science **340**, 1307 (2013).